HHS Public Access

Author manuscript

Nat Neurosci. Author manuscript; available in PMC 2020 November 06.

Published in final edited form as:

Nat Neurosci. 2011 April ; 14(4): 519–526. doi:10.1038/nn.2767.

Optical quantal analysis of synaptic transmission in wild-type and *rab3*-mutant *Drosophila melanogaster* motor axons

Einat S Peled[1], **Ehud Y Isacoff**[1,2,3]

[1]Department of Molecular and Cell Biology, University of California, Berkeley, California, USA.

[2]Helen Wills Neuroscience Institute, University of California, Berkeley, California, USA.

[3]Physical Bioscience Division, Lawrence Berkeley National Laboratory, Berkeley, California, USA.

Abstract

Synaptic transmission from a neuron to its target cells occurs via neurotransmitter release from dozens to thousands of presynaptic release sites whose strength and plasticity can vary considerably. We report an *in vivo* imaging method that monitors real-time synaptic transmission simultaneously at many release sites with quantal resolution. We applied this method to the model glutamatergic system of the *Drosophila melanogaster* larval neuromuscular junction. We find that, under basal conditions, about half of release sites have a very low release probability, but these are interspersed with sites with as much as a 50-fold higher probability. Paired-pulse stimulation depresses high-probability sites, facilitates low-probability sites, and recruits previously silent sites. Mutation of the small GTPase Rab3 substantially increases release probability but still leaves about half of the sites silent. Our findings suggest that basal synaptic strength and short-term plasticity are regulated at the level of release probability at individual sites.

An individual neuron can form thousands of contacts with multiple pre- and postsynaptic cells. Synaptic transmission in a neuronal network is shaped by the collective transmission properties of these individual contact sites. Transmitter release can vary considerably in strength and plasticity among the sites[1-3], providing great flexibility in the modulation of synaptic strength during development, plasticity in the mature network, or short-term adjustments of synaptic output levels. To understand these processes it is essential to gain detailed knowledge of the transmission properties and dynamics of individual release sites, yet efforts to elucidate these properties have faced several technical challenges.

Electrophysiological studies typically report the summed synaptic transmission of multiple sites and cannot pinpoint the release properties of specific individual sites. Nevertheless, carefully designed experiments in a variety of preparations[3-7] have made it possible to infer that release probabilities vary considerably between individual release sites.

Correspondence should be addressed to E.Y.I. (ehud@berkeley.edu).

AUTHOR CONTRIBUTIONS

E.S.P. carried out experiments and data analysis. E.Y.I. supervised the project. E.S.P. and E.Y.I. wrote the manuscript.

COMPETING FINANCIAL INTERESTS

The authors declare no competing financial interests.

Note: Supplementary information is available on the Nature Neuroscience website.

Fluorescence microscopy has been used to image both synaptic vesicle cycling with FM dyes[8-11] (a correlate of transmitter release) and Ca^{2+} entry into dendritic spines with chemical indicators[12-14] (an optical report of the activation of postsynaptic NMDA receptors). These studies, in cell culture and in brain slice, show that release probabilities of different presynaptic boutons vary over a wide range and that short-term plasticity modulates transmission properties independently at each bouton. Although much has been revealed by these approaches, a straightforward quantal analysis of synaptic activity has not been reported so far. Owing to technical constraints associated with the various imaging methods, experiments have usually been limited to either the measurement of average cumulative changes in fluorescence, induced by hundreds of action potentials, or higher-resolution, single-action-potential imaging of only a handful of synaptic release sites. Additionally, the complexity of neuronal networks makes it difficult to identify release sites that connect a specific pair of cells, complicating the analysis of the origin of variability between sites.

Here we report an approach that images synaptic transmission with quantal resolution at hundreds of release sites, *in vivo* at the *D. melanogaster* larval neuromuscular junction (NMJ). In this model glutamatergic system, which resembles central synapses in vertebrates at the molecular level[15], a few axon branches form tens to hundreds of boutons[16], with each bouton containing up to 50 transmitter release sites[17], providing a large collection of sites that together mediate transmission between the axon and its one muscle fiber target cell. We found that basal release probability can vary by as much as 50-fold between release sites, from a low release probability (<0.01) at many sites to a high release probability (>0.5) at a minority of the sites. Low- and high-probability sites can be located side by side in the same bouton, but distal boutons have a higher proportion of high-probability sites. Paired-pulse stimulation facilitates low-probability sites and depresses high-probability sites without altering transmission amplitude.

We examined transmission in a mutant of Rab3, a synaptic vesicle–associated small GTPase involved in the regulation of vesicle release[18,19]. Knockout in mouse has shown that Rab3 regulates exocytosis[20] and functions to increase release probability of a subset of synaptic vesicles[21]. Recently, a mutation of the *D. melanogaster rab3* has been shown to concentrate presynaptic Ca^{2+} channels, electron-dense T-bars and the active-zone protein Brp[22] (the *D. melanogaster* ortholog of CAST) in about one-third of the available active zones, leaving remaining active zones devoid of these presynaptic components[23]. We found that synaptic transmission in *rab3* mutants occurs only from the subset of active zones that contain Brp, with higher release probability from sites with more Brp. Additionally, the *rab3* mutation alters the global organization of transmission strength: whereas in wild type high-probability sites are disproportionately concentrated in distal boutons, in mutant NMJs they are evenly distributed along the axonal branch.

RESULTS

SynapGCaMP2 is a postsynaptically targeted Ca^{2+} sensor

To image synaptic activity in the *D. melanogaster* larval NMJ we generated a fly line that expresses the genetically encoded Ca^{2+} sensor GCaMP2 (ref. 24) in the muscles of transgenic larvae. GCaMP2 has reported K_d values in the submicromolar range, provides a

useful combination of signal-to-noise ratio, dynamic range and kinetics[24,25], and is an improvement over earlier genetically encoded Ca^{2+} sensors. The sensor was targeted to the muscle postsynapse by fusion to the integral membrane protein CD8 at its N-terminal end and the PDZ interaction domain of the Shaker K^+ channel at its C-terminal end, as has been done[26] with the earlier Ca^{2+} sensor Cameleon[27]. This method of Ca^{2+} sensor targeting enables optical imaging of Ca^{2+} influx through postsynaptic glutamate receptors. The high signal-to-noise ratio of GCaMP2, together with fast-scanning confocal imaging, allowed us to image postsynaptic responses to glutamate release from single release sites in response to both single presynaptic action potentials (Fig. 1) and spontaneous quantal release (Fig. 2).

We monitored synaptic activity at the NMJ formed on ventral longitudinal muscle fiber 4, which is innervated by three motor axons forming boutons of type Ib (big), Is (small), and II[28]. Our targeted GCaMP2 sensor, which we named SynapGCaMP2, was localized to the postsynaptic muscle membrane and outlined the presynaptic axonal branches and boutons of both the type Ib and type Is nerve terminals (Fig. 1a and Supplementary Movie 1). We focused on synaptic transmission of type Ib boutons because of their higher levels of basal fluorescence.

SynapGCaMP2 reports Ca^{2+} influx with quantal resolution

In response to a single presynaptic action potential we observed a synchronous increase in SynapGCaMP2 fluorescence in multiple small spots along the axonal branch (Fig. 1b), as expected for Ca^{2+} influx through postsynaptic glutamate receptors, which are clustered opposite release sites[29]. The time course of the fluorescence change (ΔF) was slow, as has been shown for a variety of sensors based on fusions of a fluorescent protein with calmodulin[25], rising to a peak in ~50 ms and decaying by half in ~100 ms (Fig. 1c and Supplementary Fig. 1). The ΔF trace of a single spot in response to a single presynaptic action potential was large and measurable, and closely resembled the average ΔF trace of many spots in response to many action potentials (Fig. 1c and Supplementary Fig. 1). Repeated presynaptic stimulation at a low frequency (0.06 Hz), to determine the properties of basal transmission, elicited punctate rises in postsynaptic Ca^{2+} that differed in spatial pattern from one action potential to the next (Fig. 1b and Supplementary Movie 1).

To test how accurately the evoked ΔF spots report on neurotransmitter release we examined spontaneous activity in the NMJ. Miniature excitatory postsynaptic potentials (mEPSPs), evoked by the spontaneous fusion of synaptic vesicles, occurred at a low frequency (4 ± 0.4 Hz, n = 9 NMJs) in our standard recording solution. For easier analysis we therefore initially used a high-sucrose recording solution (see Online Methods), which elevated mEPSP frequency by about four-fold (to 15 ± 2 Hz, n = 7 NMJs; Fig. 2a). The barrage of mEPSPs was accompanied by individual ΔF spots in SynapGCaMP2 images (Fig. 2b and Supplementary Movie 2). Each ΔF spot could be associated with an individual mEPSP, according to its timing (Fig. 2a-c). We found that the spot imaging amplitude ($\Delta F/F$) was correlated with mEPSP amplitude (Fig. 2d). These observations indicate that our imaging method has a single-vesicle (quantal) resolution and that $\Delta F/F$ can be used to estimate transmission strength.

The stimulation-evoked ΔF spots were similar to spontaneous ΔF spots in terms of both spatial spread and $\Delta F/F$ values (Fig. 3a-d). Here we made the comparison in normal recording solution, where spontaneous ΔF spots were occasionally detected after stimulation-evoked ΔF spots. We examined a large number of evoked events and a small number of spontaneous events from the same preparation ($n = 461$ evoked, $n = 15$ spontaneous) and found that the two share the same wide range of $\Delta F/F$ values (Fig. 3d). For a more accurate comparison we examined spontaneous and evoked ΔF spots that occurred at the same release site. We found that an individual site by itself can have a wide range of evoked $\Delta F/F$ values (Fig. 3e). Spontaneous $\Delta F/F$ values occurred at both the low and high ends of the evoked $\Delta F/F$ values at an individual site (Fig. 3e; in $n = 10$ release sites of four NMJs, the ratio of spontaneous to evoked mean $\Delta F/F$ values was 1.13 ± 0.20). These results suggest that, at low stimulation frequencies, action potentials that evoke release primarily release one synaptic vesicle per release site.

Variability in release probability and silent active zones

As we noted earlier, repeated single-action-potential stimulation trials led to a different set of ΔF spots in each trial (Fig. 1b and Supplementary Movie 1). The number of spots fluctuated about a stable value, in keeping with a stable excitatory postsynaptic current (EPSC) amplitude (Supplementary Fig. 2). We found that the average number of ΔF spots detected were consistent with the quantal content determined by electrophysiology: >90% of release events within the field of view were detected by SynapGCaMP2 imaging (Supplementary Table 1).

We constructed maps of release probability in the NMJs by counting the number of times each pixel participated in response to nerve stimulation (Figs. 4a and 5a). These maps showed that transmission occurs in multiple spots within each of the boutons along the axon branch. Some of the spots transmit frequently, with release probabilities as high as 0.5, whereas others transmit infrequently, with release probabilities as low as 0.01. To compare the SynapGCaMP2 release probability maps to locations of active zones in the NMJ, we stained the preparations for the active zone protein Brp (Fig. 4b). This showed that a substantial number of presynaptic active zones have little or no response to nerve stimulation. By comparing the number of Brp puncta to the number of identified transmission spots in the preparations, we deduced that 44 ± 7% of Brp puncta have a release probability <0.02 ($n = 4$ NMJs, 657 Brp puncta). The large contrast in probability between release sites is notable for multiple contacts of a single axon branch onto a single postsynaptic target.

We observed an overlap between transmission sites and Brp puncta (Fig. 4c), although the high density of Brp puncta and the fact that many of them were virtually silent precluded an unambiguous one-to-one assignment. In four boutons tested, we found the correlation between the sites of transmission and the Brp puncta to be 0.33 ± 0.04. Although this value of correlation is low, it is higher than what we would expect to obtain by chance, or random overlay of the two dense patterns, because rotating the Brp images by 180° reduced the correlation value to 0.23 ± 0.03 ($P < 0.03$, paired t test). We found an unambiguous correlation in a mutant with a lower density of Brp puncta (see below).

Variability within boutons and along the axon

Release probability maps typically showed a small number of high-probability sites at each NMJ (Figs. 4a and 5a). The distribution of release probabilities was skewed toward lower values and had a median value of 0.07 (Fig. 5b). Probabilities >0.2 were found in only 10% of the release sites, indicating that a small number of release sites can dominate the basal transmission of the NMJ. The spatial arrangement of high- and low-probability release sites was notable in that, within the same bouton, high-probability sites were often located within ~1.5 μm of low-probability sites (see for example, Figs. 4a and 5a). More globally, we found that the distribution of low- and high-probability release sites was nonuniform along the length of the axon. Boutons at the end of an axon branch contained a larger proportion of high-probability sites (Fig. 5c) and had more ΔF spots per action potential (Fig. 5d). This spatial distribution of release probabilities is consistent with previous observations with low-resolution imaging showing that average synaptic strength per bouton is greater for boutons situated at the end of the motor axon[26].

The mechanism underlying the uneven distribution of synaptic strength along the axonal branch is not known. Although action potential amplitude could be larger at end boutons[17], and presynaptic Ca^{2+} influx is usually higher at these locations[26,30], other factors must dominate because even in end boutons the majority of sites have a low release probability. To address this, we examined the spatial distribution of spontaneous release events along the axon. In this analysis we again used sucrose-induced mEPSPs (as in Fig. 2), because their higher frequency of occurrence allowed us to collect a large enough number of events for statistical analysis. A small fraction of release sites showed sucrose-induced miniatures at frequencies as high as 0.16 Hz, yet the majority of sites had far lower release frequencies and could be directly compared to evoked release (see Supplementary Text for discussion of possible vesicle depletion). We found that the frequency of mEPSP-associated sucrose-induced ΔF spots was higher at distal boutons than at proximal and middle boutons (Fig. 6a,b). Given that these release events occur independently at each release site, and are not triggered by an action potential, this finding suggests that release probability is determined at the level of individual release sites.

Paired-pulse facilitation and depression in the NMJ

Having observed a marked contrast between the probabilities of basal transmission at different release sites, we next asked how probability changes under conditions of short-term plasticity[31]. Studies in a variety of preparations have shown that synapses with a high release probability tend to depress, whereas low-probability synapses tend to facilitate during repetitive stimulation[1,2,10,14,32,33]. We therefore examined the effect of paired-pulse stimulation on release probabilities and transmission amplitudes in the NMJ. On average, paired-pulse stimulation with an interpulse interval of 50 ms yielded a modest facilitation of the number of evoked ΔF spots (pulse 2 / pulse 1 = 1.43 ± 0.10, n = 7 NMJs) and a similar facilitation in the recorded EPSCs (pulse 2 / pulse 1 = 1.34 ± 0.15, n = 5 NMJs) under conditions in which only the type Ib axon was stimulated (see Supplementary Fig. 3).

We found little overlap between sites that transmitted in response to the first pulse and those that transmitted in response to the second (Fig. 7a and Supplementary Movie 3): 95% of

second-pulse Δ*F* spots occurred in sites that did not participate in the first-pulse response. The rarity of transmission during both pulses can be accounted for by the low release probabilities (median probability of 0.07), which make it improbable (<1% chance, on average) that a first-pulse Δ*F* spot will be followed by a second-pulse Δ*F* spot at the same site.

The overall increase in number of Δ*F* spots upon second-pulse stimulation occurred along the entire axon branch (Fig. 7b). Occasionally we observed first-pulse low-probability release sites that had a large increase in probability in the second pulse (Fig. 7b). The opposite was true for high-probability release sites, which tended to depress in response to the second stimulation pulse (Fig. 7c and Supplementary Fig. 4a). Paired-pulse stimulation therefore leads to a mixture of facilitation and depression (Supplementary Fig. 4b): low-probability sites increase release, whereas higher-probability sites decrease release (Fig. 7c). Because low- and high-probability sites can be situated close to one another, even neighboring release sites can have opposite short-term plasticity.

In principle, paired-pulse stimulation could alter the magnitude of transmission by changing the number of vesicles released by a release site. However, we found no evidence for such an effect: Δ*F/F* values of successful responses evoked by the first and second pulse in the pulse pair were very similar. Across many release sites, first- and second-pulse Δ*F/F* values showed the same range (Fig. 7d), and comparison of first- and second-pulse Δ*F/F* values within the same release site yielded similar results (Supplementary Fig. 5). Thus, short-term plasticity at the *D. melanogaster* NMJ is brought about by changes in release probability and not in the amount of neurotransmitter released by each release site when it is active. This is in contrast to earlier imaging analysis of NMDA receptor transmission in CA1 pyramidal neurons in hippocampal slice, in which part of paired-pulse facilitation is accounted for by multivesicular release[13]. However, our results are consistent with electrophysiological measurements in hippocampal slice using minimal stimulation in which paired-pulse facilitation could be accounted for by changes in release probability under univesicular release[34,35].

Quantal analysis of transmission in *rab3*-mutant NMJs

We next examined a mutant for the synaptic-vesicle associated small GTPase Rab3, which has a role in the regulation of structure and function of active zones[23]. *rab3*-mutant NMJs contain a slightly smaller number of active zones than their wild-type counterparts. All mutant active zones seem capable of synaptic transmission, as they contain clusters of synaptic vesicles and are opposed by glutamate receptors. Yet, in mutant NMJs essential presynaptic proteins (Ca^{2+} channels, electron-dense T-bars and Brp), normally associated with all active zones, are present in only a subset of 'enriched' active zones[23]. Using SynapGCaMP2 imaging, we found that synaptic activity in the *rab3*-mutant NMJs occurs only at the enriched active zones. Maps of release probability (Fig. 8a) showed that the density of transmission spots was reduced by half in the mutants (transmission spot density = 0.23 ± 0.01 spots μm^{-2}, $n = 4$ NMJs, in *rab3* mutants, versus 0.47 ± 0.06 spots μm^{-2} in wild type, $n = 5$ NMJs; $P < 0.007$, independent *t*-test). Post-hoc staining for Brp showed a good match between the location of sites of transmission and Brp puncta (Fig. 8b) and a

correlation between release probability from each site and the site's level of Brp (Fig. 8c). Indeed, >90% of identified transmission sites (89 of 96 sites in two NMJs) were colocalized with a Brp punctum. In the *rab3*-mutant NMJs, 43 ± 5% (n = 325 Brp puncta in four NMJs) of the Brp puncta had very low release probability (<0.02), a percentage similar to that found in wild-type NMJs.

Evoked EPSCs were larger by ~50% in the *rab3* mutants in 1.5 mM external Ca^{2+} (at a holding potential of −100 mV, *rab3* mutants, 87 ± 12 nA, n = 12; wild type, 57 ± 4nA, n = 16; $P < 0.02$, independent t-test). This indicates that the smaller number of enriched active zones together release more neurotransmitter from the *rab3*-mutant motor axon than do the larger number of release sites in the wild-type axon, suggesting that the mutation increases single-site release probability and/or the amplitude of single release events. A decrease in short-term facilitation in *rab3* mutants has been reported[23], suggesting an increased release probability. Our single-transmission-site analysis provided direct evidence that this is the case. Although, as in wild type, there were more sites of low release probability in *rab3*-mutant NMJs, the mutants showed a marked shift in the probability distribution toward higher values (Fig. 8d). The higher mutant release probabilities are consistent with the finding that the mutant active zones frequently contain multiple electron-dense T-bars[23] (see Supplementary Text).

Sites of higher release probability corresponded to higher Brp levels (Fig. 8c), which are correlated with larger glutamate receptor clusters[36]. The higher-probability sites can therefore be expected to elicit larger postsynaptic responses, or larger transmission amplitudes. Indeed, we found that $\Delta F/F$ value and release probability were correlated in *rab3*-mutant and wild-type NMJs (Fig. 8e). In wild-type NMJs ~90% of release sites have probability <0.2. The higher $\Delta F/F$ values in Figure 8e are therefore rarely observed. In contrast, the higher prevalence of high-probability sites in mutant NMJs (Fig. 8d) shifts the distribution of $\Delta F/F$ toward larger values (Fig. 8f).

Aside from the alterations in active zone structure and local transmission properties described so far, we found that the absence of Rab3 had a global effect on the distribution of release probability along the length of the axon branch. In wild-type NMJs distal boutons contain more high-probability transmission sites (Fig. 5c). In contrast, *rab3*-mutant NMJs had even distribution along the axon branch of high-probability spots (Fig. 8a) and responding active zones per action potential (Fig. 8g). Because the presence of Rab3 in wild-type is associated with higher transmission at distal boutons and its absence in the *rab3* mutant is associated with globally elevated transmission, we wondered whether the Rab3 protein is normally excluded from distal boutons. However, staining of wild-type NMJs for Rab3 showed no difference in the level of Rab3, or for that matter Brp, along the axon branch (Supplementary Fig. 6), indicating that the involvement of Rab3 in establishing the global distribution of release probabilities cannot be accounted for by the simple effect of local concentration.

DISCUSSION

We have combined a new postsynaptically targeted Ca^{2+} sensor, SynapGCaMP2, with fast-scanning confocal microscopy to image glutamatergic transmission in the *D. melanogaster* larval NMJ. The method provides simultaneous quantal resolution for hundreds of active zones in dozens of boutons along a long axon *in vivo*. The simultaneous information on the release properties of such a large collection of release sites makes it possible to examine how both spontaneous miniature release events and events evoked by a single action potential are distributed in time and space along the axon, to compare the release properties of the two kinds of events, and to study the changes in release in a paradigm of short-term plasticity.

Our *in vivo* observations confirm earlier deductions from less direct experimental techniques that transmitter release properties and short-term facilitation can differ between the release sites of a single axon[1-3,5,10,37], that there is a correlation between the probability of evoked release and the frequency of spontaneous release[38], and that, in the *D. melanogaster* NMJ, transmission is stronger at distal boutons[26]. The optical quantal analysis of our imaging and analysis methods enabled us to examine the collection of hundreds of release sites that make up the NMJ and determine the release probability and amplitude of each one of them. In wild-type NMJs, we find that release sites can differ in their release probabilities and transmission amplitudes, although the difference in transmission amplitudes is only significant for a small number of sites of exceptionally high release probabilities. Additionally, we find that the short-term modulation of overall synaptic strength is achieved by a change in the balance of release probabilities that leads to an altered spatial arrangement of strong and weak release sites and not by changes in the amount of neurotransmitter released when a site is active.

In hippocampal neurons, release probability is correlated with active-zone size[39,40]. In the *D. melanogaster* NMJ, more glutamate receptors cluster opposite larger presynaptic active zones[36], suggesting that the same correspondence between active-zone area and release probability could hold. However, we find no clear relation between active-zone size and basal release probability in wild-type NMJs, suggesting that other source or sources of variability dominate. Indeed, of the many hundreds of active zones present along an axon branch only a small minority has a high basal release probability, and these are disproportionately concentrated at distal boutons, despite uniformity in the density of presynaptic active zones.

Our observations show that a substantial number of release sites have such low basal release probability that no activity is detected, that is, they are effectively silent. Some of these sites become active when presented with a second stimulation pulse a short time after the first stimulation, confirming that they are functional and within our detection capabilities. These observations are consistent with earlier evidence indicating that whereas some release sites are more active, releasing transmitter in response to single action potentials, others are reluctant, participating in synaptic activity only under more demanding conditions that involve high-frequency presynaptic activity[32,41].

SynapGCaMP2 was targeted to the muscle postsynapse to report Ca^{2+} influx via glutamate receptors. This postsynaptic measure seems to give an accurate representation of presynaptic neurotransmitter release in that the number of detected ΔF spots agreed with the calculated quantal content in wild-type preparations and the altered presynaptic organization of the *rab3* mutants matched the pattern of postsynaptically imaged activity. Some transmission events could be too small, because of a paucity of postsynaptic receptors, to be detected by our method and, therefore, fall into the group of 44% of sites that we assign as functionally silent. However, a previous study found that glutamate receptor subunit composition and numbers are not correlated with average postsynaptic transmission strength in wild-type NMJs[26]. If there is a postsynaptic mechanism that affects the amount of postsynaptic Ca^{2+} influx it would therefore probably involve post-translational modifications that affect glutamate receptor function but are not necessarily detected by immunohistochemistry. One such mechanism could be the suggested PKA regulation of the function of the *D. melanogaster* glutamate receptor subunit DGluRIIA[42].

It remains to be determined how different release properties are established. Our work demonstrates that the mechanisms involved in this process operate differentially even for closely spaced release sites within the same bouton. Yet the resulting arrangement of release properties along the axonal branch is not random, as more high-probability release sites are located at distal boutons. These results suggest the existence of both local intrabouton regulation at the level of single release sites and global interbouton regulation at the level of the entire axon.

The small GTPase Rab3 is involved in the regulation of neurotransmitter release[18-21]. Recently, a study in *D. melanogaster* has shown that in *rab3*-mutant NMJs essential presynaptic proteins are concentrated in a subset of the available active zones[23], suggesting either a separate additional role of Rab3 in presynaptic organization, or that the effect of Rab3 on release probability is achieved via its recruitment of presynaptic proteins to active zones. We found that in *rab3*-mutant NMJs transmission occurs exclusively at the presynaptically enriched active zones, which are elevated in both release probability and transmission amplitude. Notably, the absence of Rab3 not only alters the size and release properties of individual active zones but also affects the distribution of release probabilities along the axon branch. In contrast to wild-type NMJs, where there are more high-probability release sites in distal boutons, the distribution of high-probability sites is equal throughout the axon branch in the mutant NMJs. This is not because of an inhomogeneity in Rab3 distribution in wild-type axons, but perhaps it reflects a spatial inhomogeneity in Rab3 regulation, for example in the regulation of the GTPase activity of Rab3.

METHODS

Methods and any associated references are available in the online version of the paper at http://www.nature.com/natureneuroscience/.

ONLINE METHODS

DNA construct and flies.

To target the Ca^{2+} sensor GCaMP2 to the muscle postsynapse, we started with the Synapcam 3.1 DNA construct MHC-CD8-*Cam3.1*-SH (ref. 26). GCaMP2 (a gift from J. Nakai, RIKEN Brain Science Institute, Wako-shi, Saitama, Japan) was amplified with *SpeI* primers and inserted into the *SpeI* site of the Synapcam 3.1 construct, exchanging *Cam3.1* for GCaMP2 to generate the SynapGCaMP2 construct MHC-CD8-GCaMP2-SH. Transgenic flies were made using standard germline transformation by embryo injection (BestGene).

rab3 mutant flies were obtained from A. DiAntonio[23] (Washington University School of Medicine). The mutants were $rab3^{rup}$ and Df(2R)ED2076 (*rab3* mutation and the corresponding second-chromosome deficiency).

Third instar larvae were used in all experiments. The following genotypes were used: wild type, w1118; +; SynapGCaMP2/+ and *rab3* mutant, w1118; $rab3^{rup}$/Df(2R)ED2076; SynapGCaMP2/+.

Electrophysiology.

Larvae were dissected in HL3 solution and then washed with the solution used for recording. HL3 solution contained 70 mM NaCl, 5 mM KCl, 1.5 mM $CaCl_2{\cdot}2H_2O$, 20 mM $MgCl_2{\cdot}6H_2O$, 10 mM $NaHCO_3$, 5 mM trehalose, 115 mM sucrose, 5 mM HEPES, pH 7.2. Stimulation-evoked recordings (single-action-potential and paired-pulse stimulation) were done in high-Mg^{2+} HL3 solution (HL3 solution with 25 mM $MgCl_2{\cdot}6H_2O$). We found that the higher Mg^{2+} concentration slightly reduced release probabilities in the NMJ, allowing for easier detection of individual release events and separation of release sites. Furthermore, muscle contractions were almost never present in the high-Mg^{2+} solution. Recordings of sucrose-induced spontaneous activity were done in high-sucrose HL3 solution (HL3 solution with 269 mM sucrose and 5 mM $CaCl_2{\cdot}2H_20$). Ca^{2+} concentration was increased to augment the ΔF signal, because fluorescence was reduced by the elevated sucrose.

Recordings were done with an AxoClamp-2A amplifier (Molecular Devices) on ventral longitudinal abdominal muscle 4 at segments A2–A4 of third instar larvae. Recording electrodes contained 3M KCl and had resistances in the range of 15–25 M. Only muscles with resting potential below −60 mV and membrane resistance >4 M were chosen for study. Data were filtered at 1 kHz and recorded at 5 kHz, using a Digidata 1322A interface and Clampex 8.0 software (Molecular Devices).

For stimulation-evoked recordings (single-action-potential and paired-pulse stimulation), muscles were voltage clamped at −80 mV during waiting periods and at −100 mV during stimulation and image acquisition times. For repeated trials of nerve stimulation by a single action potential, the nerve was stimulated at 0.06 Hz during continuous imaging experiments or at 0.125 Hz during two-image acquisition experiments (see imaging details below). For paired-pulse stimulation, the nerve was stimulated with an interpulse interval of 50 ms, at a rate of 0.06 Hz. Each single nerve stimulus lasted 0.2–1 ms, and stimulus time and amplitude were adjusted to ensure recruitment of both Is and Ib axonal terminals.

For sucrose-induced spontaneous activity measurements the amplifier was kept in Bridge mode, to reduce electronic noise. The first recording electrode was used to monitor V_m and the second to inject current so as to keep V_m at −100 mV. The amplitude of injected current was adjusted manually at the beginning of each experiment and typically had to be readjusted every several minutes.

To verify that SynapGCaMP2 imaging reports Ca^{2+} influx via postsynaptic glutamate receptors, we desensitized glutamate receptors in the NMJ by the application of ≥2 mM glutamate in HL3 (2 mM or 5 mM l-glutamic acid monosodium salt hydrate, Sigma). This blocked both the EPSC and the SynapGCaMP2 response.

SynapGCaMP2 fluorescence imaging.

Fluorescence images were acquired with the Zeiss LSM 5 LIVE fast scanning confocal microscope and a 63×/1.0 water immersion objective (Carl Zeiss). Slit aperture was set for an optical slice thickness of ~3.5 μm. Pixel size was 0.31 × 0.31 μm^2 and images were saved at 12-bit depth. Fluorescence excitation and detection were done with a 488-nm laser line and 495-nm LP emission filter, respectively. A single confocal plane slice of the NMJ was imaged continuously at rates of 50 or 100 frames per second (f.p.s.), for a period of 0.25–1 s for each trial, depending on the nerve-stimulation protocol (rates, 50, 100 and 50 f.p.s.; total scan times, 600, up to 640 and 500–1,000 ms for single-pulse stimulation, paired-pulse stimulation and sucrose-induced spontaneous activity, respectively). Multiple imaging scans (with the concomitant nerve stimulation) were done at intervals of 16 s between the start of one scan and the next. At least 37 (but typically ~100) scans were included in each recording. Several of the evoked stimulation recordings were done in a different image acquisition mode. Instead of continuous image acquisition, only two images were acquired: a baseline image obtained ~1 s before nerve stimulation and a response image at the time of the peak fluorescence response. Image scanning times were 40 ms (each image was an average of two images, taken at 50 f.p.s.). The two imaging modes yielded the same results.

Image analysis.

Before analysis, all images were filtered (Gaussian low-pass filter), to reduce high-frequency noise. For automatic detection of stimulation-evoked ΔF spots, in continuous imaging mode, we first manually identified several (typically >30) ΔF spots (across >10 release sites and several stimulation trials). These were used for generating ΔF traces (trace of ΔF over time), as in Supplementary Fig. 1a. The average of these ΔF traces (Supplementary Fig. 1b) was used to generate a template response trace (Supplementary Fig. 1c). A separate template response trace was determined for each set of recording conditions (scanning rate and recording solution). The amplitude of fluorescence changes (ΔF) was determined by correlating ΔF traces to the template response trace, on a pixel-by pixel basis. These pixel-by-pixel ΔF values were then used to generate ΔF response images, and ΔF images were divided by basal-fluorescence ($t = 0$) images to obtain the normalized $\Delta F/F$ values. In two-image acquisition mode ΔF response maps were generated by subtracting the first image from the second, and the normalized response maps ($\Delta F/F$) were obtained by dividing ΔF maps by the first image.

Automatic detection of sucrose-induced spontaneous activity was done as described above for the continuous imaging acquisition mode. Correlation of ΔF traces with a template trace (Supplementary Fig. 1d) was evaluated over the entire scan time, to allow detection of miniature events at any time point during the scan. Because of the slow fluorescence decay of the SynapGCaMP2 ΔF (see, for example, Supplementary Fig. 1d) we could also detect miniature events that occurred up to ~400 ms before the start of imaging acquisition. These 'miniature tails' appeared as bright spots in the first acquired image ($t = 0$) that decayed in fluorescence in subsequent images. Miniature tails were identified using a separate template trace (Supplementary Fig. 1e), equal to the decay part of the full miniature template trace. These events were included in the data set for analyzing the distribution of miniature events along the axonal branch (Fig. 6b), but could not be used for determining miniature time and amplitude.

To compare activity levels among different boutons along the axon branch (Figs. 5a, 6b and 8g), we divided axon branches into consecutive segments, roughly corresponding to one bouton each, based on the morphology of basal fluorescence along the branch (see Supplementary Fig. 8). We then counted the number of ΔF spots that occurred in each bouton throughout the duration of the experiment and normalized this count by the area of the bouton.

To construct release probability maps (such as Fig. 4a) we identified the centers of ΔF spots in response images (such as Fig. 1b) by searching for local maxima, and counted how many times out of all stimulation trials each pixel was identified as a spot center. The probability maps are color coded to show the percentage of times each pixel was identified as a ΔF spot center. The probability scale for these images was set so that its maximum reports the maximal release-site probability in the image (see below). Probability maps were filtered (Gaussian low-pass filter) for display purposes. Reported probability values were not affected by this filtering because they were determined using unfiltered data (see below).

To determine release probabilities of individual release sites, each release site was identified as an area of local maximum in the release probability map. A nine-pixel square area was assigned to each site and the number of ΔF spots that were centered in that area during all stimulation trials was counted (a ΔF spot was assigned to the nine-pixel area if its maximum response pixel was within that area). To obtain release probabilities, the total number of ΔF spots occurring at each release site was divided by the number of stimulation trials. For spontaneous activity, the total number of ΔF spots in each release site was divided by the total imaging time, to obtain the frequency of events at that site.

To determine transmission amplitudes within individual release sites (Supplementary Fig. 9), individual release sites were identified as areas of local maximum in the release probability maps. One release site was selected and a circle was drawn around its center position. Individual $\Delta F/F$ response images (as in Fig. 1b) were examined manually for ΔF spots that were centered at the location of the selected release site, allowing for a drift of one pixel in each direction. Single-release-site transmission amplitudes can be overestimated owing to overflow of Ca^{2+} influx when neighboring sites respond in the same stimulation trial. To avoid this error we included in analysis only well-isolated ΔF spots.

Immunohistochemistry.

Larvae were fixed in 4% (vol/vol) formaldehyde in HL3 solution for 20 min. The following primary antibodies were used: mouse antibody to Brp, 1:100 (Developmental Studies Hybridoma Bank); rabbit antibody to Rab3 (ref. 23), 1:1,000 (a gift from A. DiAntonio, Washington University School of Medicine, Saint Louis). Secondary antibodies, used at 1:1,000, were Alexa 647- and 532-conjugated goat anti-mouse and Alexa 647-conjugated goat anti-rabbit (Molecular Probes). Cy3-conjugated goat anti-HRP (Jackson ImmunoResearch Laboratories) was used at 1:100. Antibodies obtained from the Developmental Studies Hybridoma Bank were developed under the auspices of the US National Institute of Child Health and Human Development and maintained by the Department of Biological Sciences of the University of Iowa (Iowa City, Iowa, USA).

Images of stained preparations were acquired with the Zeiss LSM 5 LIVE fast scanning confocal microscope and a 40×/1.3 DIC oil immersion objective (Carl Zeiss). Pixel size was $\geq 0.17 \times 0.17\ \mu m^2$ and images were saved at 12-bit depth.

Analysis of immunohistochemistry images.

To determine Brp intensity at individual transmission spots (Fig. 8c), a nine-pixel square area was assigned to each transmission spot and the average value of Brp intensity within that area was calculated. The Brp intensities were binned to three equidistant levels ranging from zero to the maximal Brp intensity. Average Brp and Rab3 levels (Supplementary Fig. 6a,c) were the average intensity levels within individual boutons. Brp density (Supplementary Fig. 6b) was determined by manually counting the number of Brp puncta in each bouton.

Correlation of release probabilities to locations of Brp puncta.

When comparing Brp patterns to release-probability maps (Figs. 4 and 8b) larvae were fixed immediately after optical recording. The fixation procedure tended to stretch the preparation in one direction. Stretching was corrected using either the Matlab function cp2tform or the program warp1 (ref. 43; http://www.lifesci.sussex.ac.uk/research/cuttlefish/image_warping_software.htm). The two functions yielded similar results. Both methods aligned the live and fixed images on the basis of manual selection of pairs of matching reference points between the two images. We analyzed only preparations that required minimal stretching-correction.

To estimate the number of Brp puncta that had a postsynaptic response we manually counted the number of Brp puncta and the number of probability transmission spots in the NMJ. Large, smeared probability spots were counted as multiple spots (using the average size of well-separated spots as a guide to determine how many spots could be expected to be combined to form the smeared pattern), and Brp puncta that were closer than ~1 μm were counted as one spot, because they would not have been resolved as separate spots during SynapGCaMP2 imaging.

Statistical analysis.

Student's *t*-test was used for pairwise comparisons. Comparisons of distributions were done using the Kolmogorov-Smirnov test. Correlation between data sets was tested by calculating the correlation coefficient *r*. Reported values are mean ± s.e.m. All imaging and electrophysiology data analysis were done using custom written Matlab routines (Matlab R2007b, Mathworks). Further information is available upon request.

Supplementary Material

Refer to Web version on PubMed Central for supplementary material.

ACKNOWLEDGMENTS

We thank R.S. Zucker for helpful discussions, G. Kauwe and G. Agarwal for help generating the SynapGCaMP2 fly line, H.L. Aaron for advice on imaging and J.A. Min for help with testing fly strains. We also thank A. DiAntonio for gifts of fly strains and for the Rab3 antibody. This work was supported by US National Science Foundation grant FIBR 0623527.

References

1. Atwood HL & Karunanithi S Diversification of synaptic strength: presynaptic elements. Nat. Rev. Neurosci 3, 497–516 (2002). [PubMed: 12094207]
2. Pelkey KA & McBain CJ Differential regulation at functionally divergent release sites along a common axon. Curr. Opin. Neurobiol 17, 366–373 (2007). [PubMed: 17493799]
3. Branco T & Staras K The probability of neurotransmitter release: variability and feedback control at single synapses. Nat. Rev. Neurosci 10, 373–383 (2009). [PubMed: 19377502]
4. Redman S & Walmsley B Amplitude fluctuations in synaptic potentials evoked in cat spinal motoneurones at identified group Ia synapses. J. Physiol. (Lond.) 343, 135–145 (1983). [PubMed: 6644615]
5. Rosenmund C, Clements JD & Westbrook GL Nonuniform probability of glutamate release at a hippocampal synapse. Science 262, 754–757 (1993). [PubMed: 7901909]
6. Hessler NA, Shirke AM & Malinow R The probability of transmitter release at a mammalian central synapse. Nature 366, 569–572 (1993). [PubMed: 7902955]
7. Allen C & Stevens CF An evaluation of causes for unreliability of synaptic transmission. Proc. Natl. Acad. Sci. USA 91, 10380–10383 (1994). [PubMed: 7937958]
8. Betz WJ & Bewick GS Optical analysis of synaptic vesicle recycling at the frog neuromuscular junction. Science 255, 200–203 (1992). [PubMed: 1553547]
9. Ryan TA & Smith SJ Vesicle pool mobilization during action potential firing at hippocampal synapses. Neuron 14, 983–989 (1995). [PubMed: 7748565]
10. Murthy VN, Sejnowski TJ & Stevens CF Heterogeneous release properties of visualized individual hippocampal synapses. Neuron 18, 599–612 (1997). [PubMed: 9136769]
11. Ryan TA Presynaptic imaging techniques. Curr. Opin. Neurobiol 11, 544–549 (2001). [PubMed: 11595486]
12. Murphy TH, Baraban JM, Wier WG & Blatter LA Visualization of quantal synaptic transmission by dendritic calcium imaging. Science 263, 529–532 (1994). [PubMed: 7904774]
13. Oertner TG, Sabatini BL, Nimchinsky EA & Svoboda K Facilitation at single synapses probed with optical quantal analysis. Nat. Neurosci 5, 657–664 (2002). [PubMed: 12055631]
14. Koester HJ & Johnston D Target cell-dependent normalization of transmitter release at neocortical synapses. Science 308, 863–866 (2005). [PubMed: 15774725]
15. Budnik V & Ruiz-Cañada C The Fly Neuromuscular Junction: Structure and Function 2 2nd edn. (Elsevier Academic Press, San Diego, 2006).

16. Schuster CM, Davis GW, Fetter RD & Goodman CS Genetic dissection of structural and functional components of synaptic plasticity. I. Fasciclin II controls synaptic stabilization and growth. Neuron 17, 641–654 (1996). [PubMed: 8893022]
17. Atwood HL, Govind CK & Wu CF Differential ultrastructure of synaptic terminals on ventral longitudinal abdominal muscles in *Drosophila* larvae. J. Neurobiol 24, 1008–1024 (1993). [PubMed: 8409966]
18. Geppert M & Sudhof TC RAB3 and synaptotagmin: the yin and yang of synaptic membrane fusion. Annu. Rev. Neurosci 21, 75–95 (1998). [PubMed: 9530492]
19. Sudhof TC The synaptic vesicle cycle. Annu. Rev. Neurosci 27, 509–547 (2004). [PubMed: 15217342]
20. Schlüter OM, Schmitz F, Jahn R, Rosenmund C & Sudhof TC A complete genetic analysis of neuronal Rab3 function. J. Neurosci 24, 6629–6637 (2004). [PubMed: 15269275]
21. Schlüter OM, Basu J, Sudhof TC & Rosenmund C Rab3 superprimes synaptic vesicles for release: implications for short-term synaptic plasticity. J. Neurosci 26, 1239–1246 (2006). [PubMed: 16436611]
22. Kittel RJ et al. Bruchpilot promotes active zone assembly, Ca^{2+} channel clustering, and vesicle release. Science 312, 1051–1054 (2006). [PubMed: 16614170]
23. Graf ER, Daniels RW, Burgess RW, Schwarz TL & DiAntonio A Rab3 dynamically controls protein composition at active zones. Neuron 64, 663–677 (2009). [PubMed: 20005823]
24. Tallini YN et al. Imaging cellular signals in the heart in vivo: Cardiac expression of the high-signal Ca^{2+} indicator GCaMP2. Proc. Natl. Acad. Sci. USA 103, 4753–4758 (2006). [PubMed: 16537386]
25. Hendel T et al. Fluorescence changes of genetic calcium indicators and OGB-1 correlated with neural activity and calcium in vivo and in vitro. J. Neurosci 28, 7399–7411 (2008). [PubMed: 18632944]
26. Guerrero G et al. Heterogeneity in synaptic transmission along a *Drosophila* larval motor axon. Nat. Neurosci 8, 1188–1196 (2005). [PubMed: 16116446]
27. Miyawaki A et al. Fluorescent indicators for Ca^{2+} based on green fluorescent proteins and calmodulin. Nature 388, 882–887 (1997). [PubMed: 9278050]
28. Hoang B & Chiba A Single-cell analysis of *Drosophila* larval neuromuscular synapses. Dev. Biol 229, 55–70 (2001). [PubMed: 11133154]
29. Fouquet W et al. Maturation of active zone assembly by *Drosophila* Bruchpilot. J. Cell Biol 186, 129–145 (2009). [PubMed: 19596851]
30. Lnenicka GA, Grizzaffi J, Lee B & Rumpal N Ca^{2+} dynamics along identified synaptic terminals in *Drosophila* larvae. J. Neurosci 26, 12283–12293 (2006). [PubMed: 17122054]
31. Zucker RS & Regehr WG Short-term synaptic plasticity. Annu. Rev. Physiol 64, 355–405 (2002). [PubMed: 11826273]
32. Quigley PA, Msghina M, Govind CK & Atwood HL Visible evidence for differences in synaptic effectiveness with activity-dependent vesicular uptake and release of FM1–43. J. Neurophysiol 81, 356–370 (1999). [PubMed: 9914295]
33. Lnenicka GA & Keshishian H Identified motor terminals in *Drosophila* larvae show distinct differences in morphology and physiology. J. Neurobiol 43, 186–197 (2000). [PubMed: 10770847]
34. Stevens CF & Wang Y Facilitation and depression at single central synapses. Neuron 14, 795–802 (1995). [PubMed: 7718241]
35. Hanse E & Gustafsson B Quantal variability at glutamatergic synapses in area CA1 of the rat neonatal hippocampus. J. Physiol. (Lond.) 531, 467–480 (2001). [PubMed: 11230519]
36. Marrus SB & DiAntonio A Preferential localization of glutamate receptors opposite sites of high presynaptic release. Curr. Biol 14, 924–931 (2004). [PubMed: 15182665]
37. Branco T, Staras K, Darcy KJ & Goda Y Local dendritic activity sets release probability at hippocampal synapses. Neuron 59, 475–485 (2008). [PubMed: 18701072]
38. Prange O & Murphy TH Correlation of miniature synaptic activity and evoked release probability in cultures of cortical neurons. J. Neurosci 19, 6427–6438 (1999). [PubMed: 10414971]

39. Harris KM & Stevens JK Dendritic spines of CA 1 pyramidal cells in the rat hippocampus: serial electron microscopy with reference to their biophysical characteristics. J. Neurosci 9, 2982–2997 (1989). [PubMed: 2769375]

40. Murthy VN, Schikorski T, Stevens CF & Zhu Y Inactivity produces increases in neurotransmitter release and synapse size. Neuron 32, 673–682 (2001). [PubMed: 11719207]

41. Atwood HL & Wojtowicz JM Silent synapses in neural plasticity: current evidence. Learn. Mem 6, 542–571 (1999). [PubMed: 10641762]

42. Davis GW, DiAntonio A, Petersen SA & Goodman CS Postsynaptic PKA controls quantal size and reveals a retrograde signal that regulates presynaptic transmitter release in *Drosophila*. Neuron 20, 305–315 (1998). [PubMed: 9491991]

43. Anderson JC et al. Modular organization of adaptive colouration in flounder and cuttlefish revealed by independent component analysis. Network 14, 321–333 (2003). [PubMed: 12790187]

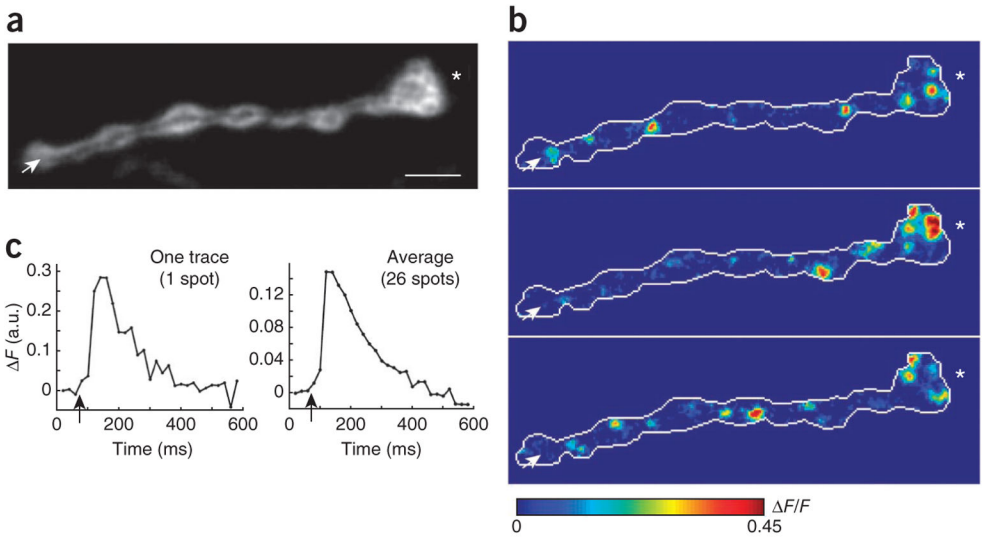

Figure 1.

Postsynaptically targeted GCaMP2 (SynapGCaMP2) reports single-action-potential, single-release-site Ca^{2+} influx. (**a**) Single-plane confocal image of basal fluorescence in the NMJ of ventral longitudinal abdominal muscle 4. (**b**) Normalized fluorescence changes in the NMJ in **a**, after three separate single-action-potential nerve stimulation trials. Scale bar, 10 μm (**a,b**). (**c**) Traces of ΔF due to a single action potential. Left, ΔF in one Ca^{2+}-influx spot. Right, average of 40 ΔF traces, obtained from 26 release sites over 10 nerve stimulation trials. Black arrows, time of nerve stimulation. Proximal and distal boutons in **a** and **b**, white arrow and asterisk, respectively.

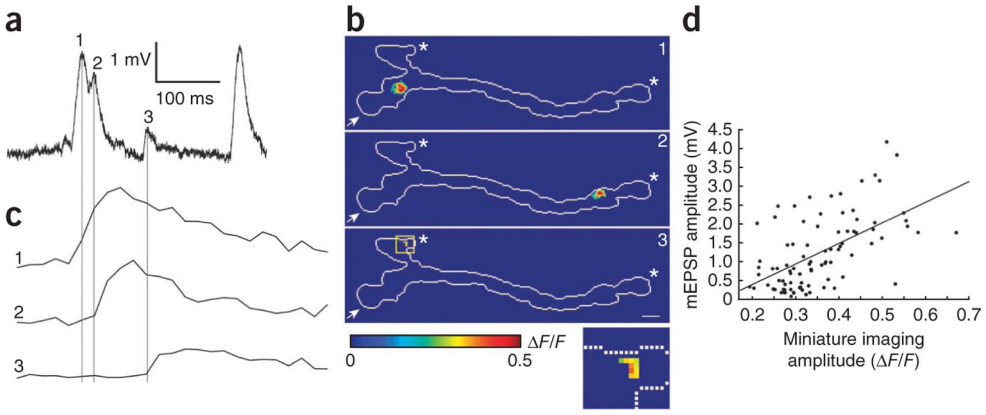

Figure 2.

SynapGCaMP2 imaging of sucrose-induced spontaneous release events. (**a,b**) mEPSPs (**a**) can be associated with spontaneous Δ*F* spots (numbered panels in **b**). Inset in bottom of **b**, higher magnification of the third release event (small Δ*F* spot in yellow square). Proximal and distal boutons, white arrow and asterisk, respectively (**b** contains two distal boutons). Scale bar, 5 μm (**b**). (**c**) Δ*F* traces (in arbitrary units) corresponding to the three spontaneous events captured in **a** and **b**. Gray vertical lines, time of mEPSP peaks in **a**. Time scale is the same as in **a**. (**d**) Correlation of miniature imaging amplitudes with mEPSP amplitudes (n = 89 events, r = 0.57; P < 0.0001, correlation analysis). All data in **a–d** were obtained from a single NMJ. Similar results were obtained from five additional NMJs (data not shown).

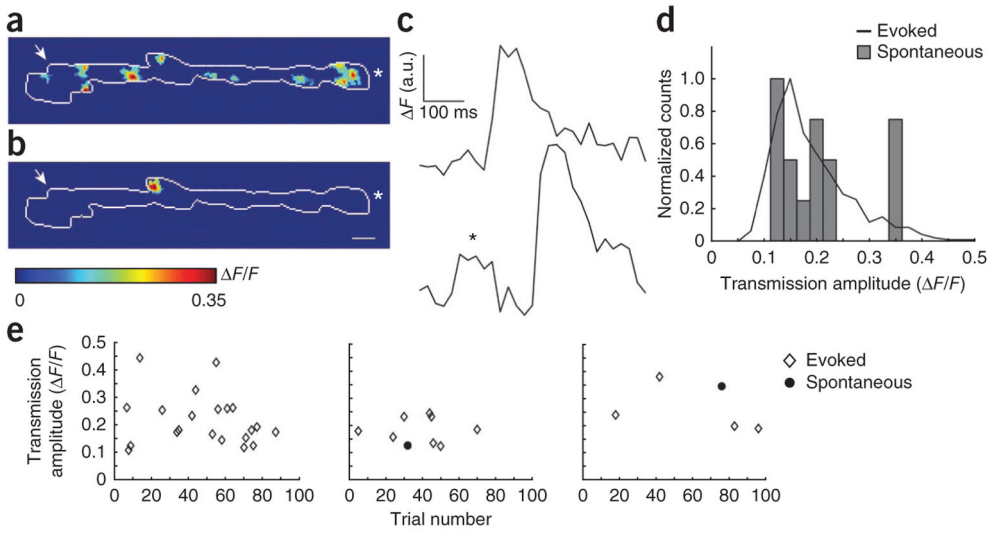

Figure 3.

Stimulation-evoked responses have same Δ*F/F* range of values as spontaneous events. (**a**) Δ*F/F* response map in response to nerve stimulation by a single action potential. (**b**) Δ*F/F* map of a spontaneous event in the same preparation. (**a,b**) Proximal and distal boutons, white arrow and asterisk, respectively. Scale bar, 5 μm. (**c**) Two examples of spontaneous Δ*F* traces in the same preparation as in **a** and **b**. Asterisk, Δ*F* response to nerve stimulation. (**d**) Distributions of evoked and spontaneous Δ*F/F* values in the same NMJ ($n = 461$ evoked events; $n = 15$ spontaneous events). (**e**) Representative examples of evoked and spontaneous imaging amplitudes within a single release site (each panel is one site). Left, stimulus-evoked Δ*F/F* values. Middle and right, spontaneous and evoked Δ*F/F* values at two other release sites.

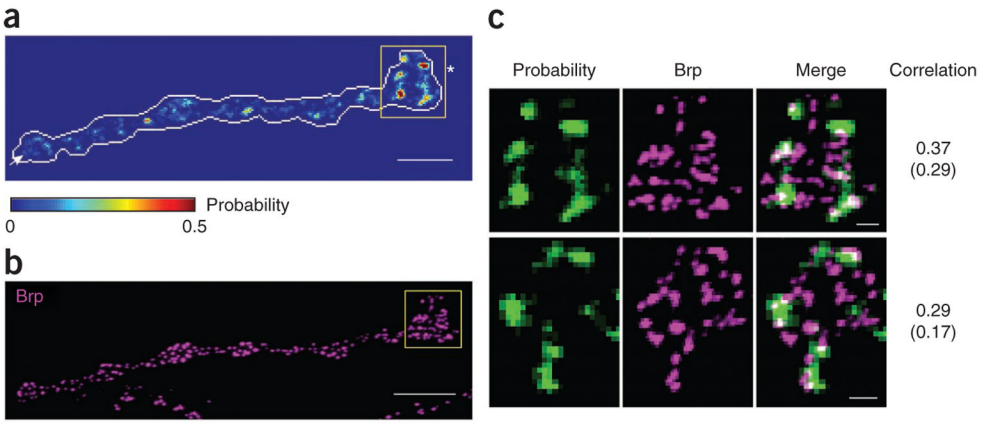

Figure 4.

Comparison of release probabilities to locations of active zones in the NMJ. (**a**) Map of aggregate release probabilities in the NMJ, showing fraction of times each release site participated in response to nerve stimulation by a single action potential (n = 101 trials). Proximal and distal boutons, arrow and asterisk, respectively. (**b**) Confocal image of the NMJ from **a**, stained for the presynaptic active-zone protein Brp. (**c**) Higher-magnification images showing overlay of probability and Brp images in two boutons. Top panels, distal bouton, surrounded by yellow squares, in **a** and **b**. Bottom panels, bouton from a different branch of the same NMJ. Numbers to right of images, value of the two-dimensional correlation between the probability and Brp patterns. Numbers in parentheses, estimated chance correlation values, obtained after rotation of the Brp patterns by 180°. Scale bars, 10 μm, **a** and **b**; 2 μm, **c**.

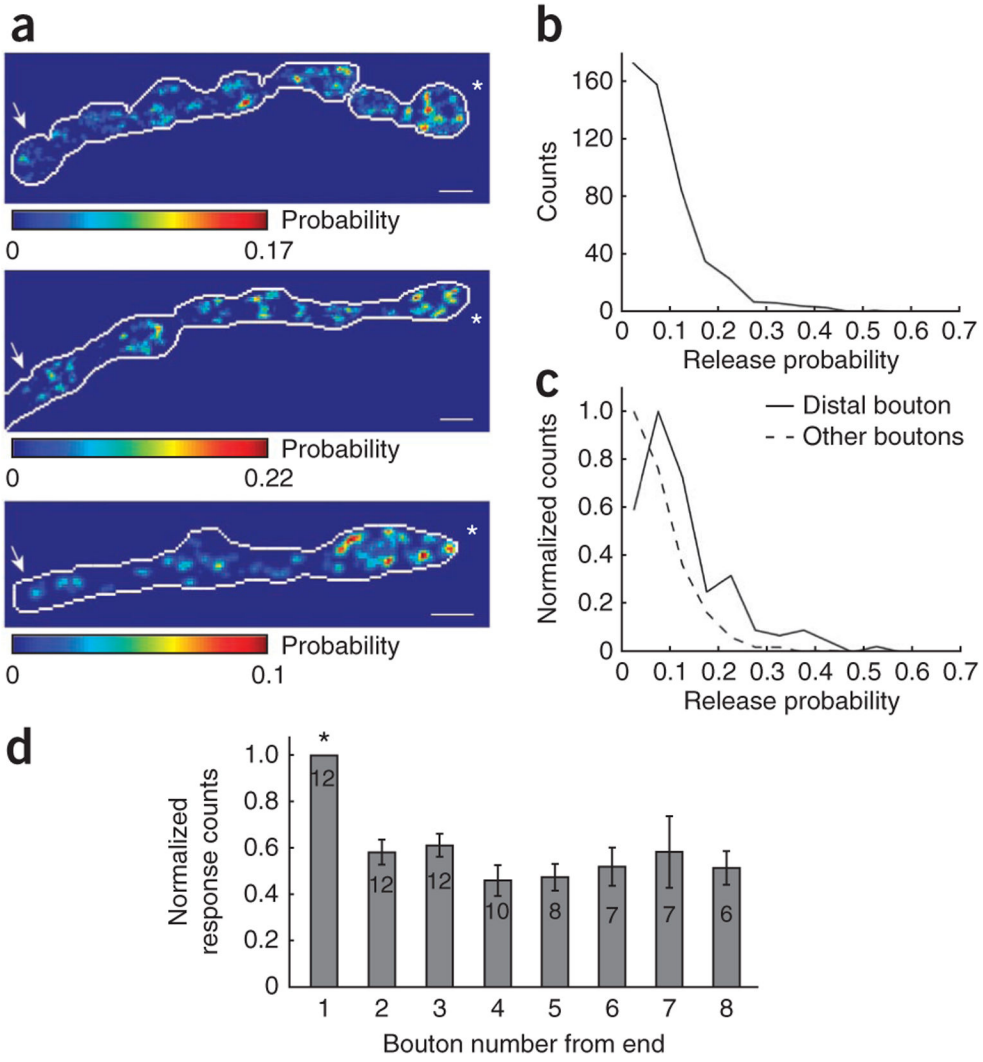

Figure 5.

The distal bouton is more active than other boutons along the axonal branch. (**a**) Examples of aggregate release probability maps in three NMJs (n = 98, 95 and 89 stimulation trials for top, middle and bottom). Proximal and distal boutons, arrow and asterisk, respectively. Scale bars, 5 μm. (**b**) Distribution of single-site release probabilities for all sites in the NMJ (n = 495 release sites, 9 NMJs). The low-release-probability counts are probably underestimated because pixels that responded only once in all stimulation trials would not have been identified as a release site (see Online Methods). (**c**) Distribution of release probabilities for sites in distal boutons and all other boutons along the axonal branch (n = 12 branches, 9 NMJs; n = 141 sites in distal boutons and 352 sites in other boutons). (**d**) Average number of ΔF spots per bouton (mean ± s.e.m.) versus bouton location from end of branch. Counts normalized by bouton area and normalized to distal bouton (bouton number 1). Numbers in bars are number of boutons averaged (n = 12 branches, 9 NMJs; *P < 0.002, paired t-test, comparing the distal bouton to each of the other boutons).

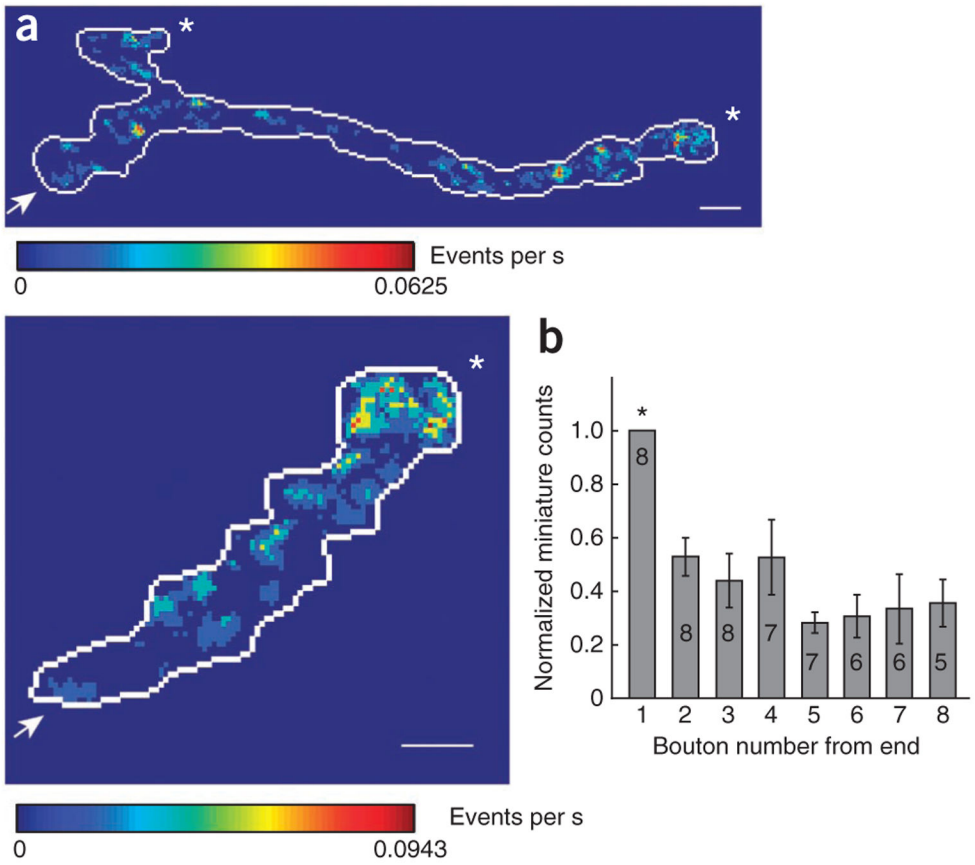

Figure 6.

The distal bouton has more spontaneous (sucrose-induced) Δ*F* spots than other boutons along the axonal branch. (**a**) Two examples of maps of the frequencies of miniature events in the NMJ (*n* = 80, 53 imaging scans for top and bottom, respectively; see Online Methods). Proximal and distal boutons, arrow and asterisk, respectively (top panel in **a** contains two distal boutons). Scale bars, 5 μm. (**b**) Average number of spontaneous Δ*F* spots per bouton (mean ± s.e.m.) versus bouton location along the branch. Counts are normalized by bouton area and normalized to distal bouton (bouton number 1) counts. Numbers in bars are numbers of boutons averaged (*n* = 8 branches, 7 NMJs; **P* < 0.0002, paired *t*-test, comparing the distal bouton to each of the other boutons).

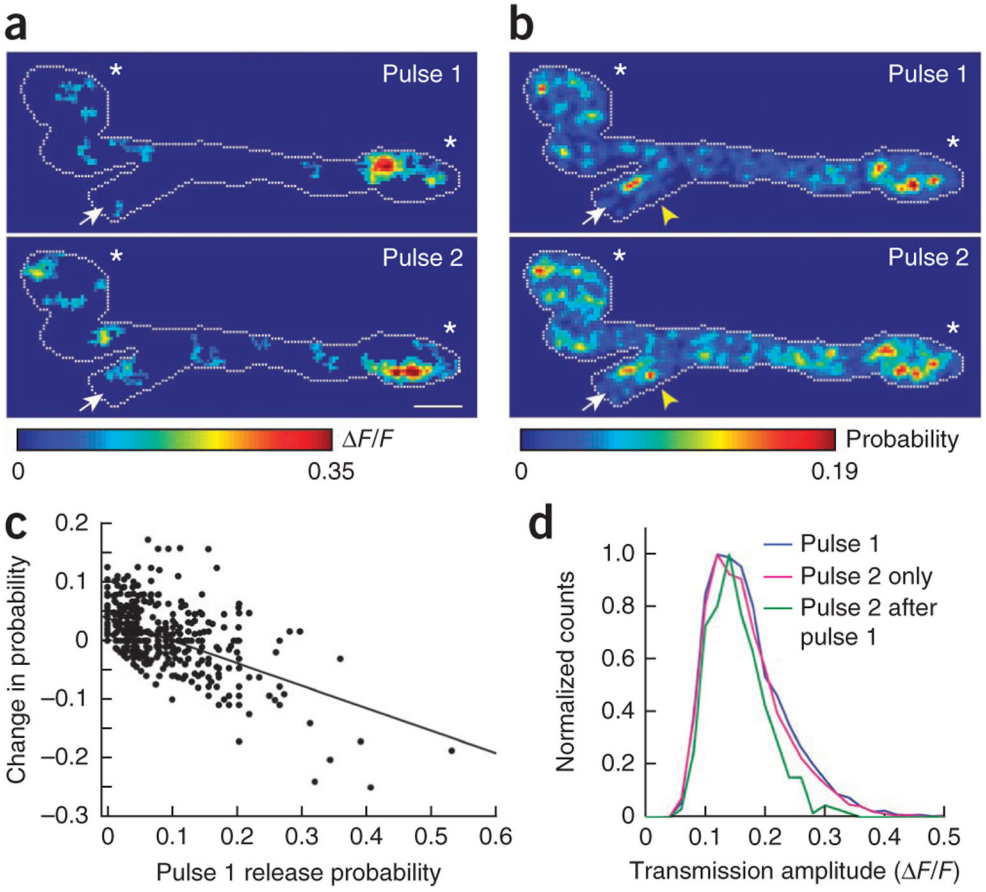

Figure 7.

Paired-pulse stimulation facilitates low-probability sites and depresses high-probability sites. (**a**) Δ*F/F* single trial response maps for pulses 1 and 2 in paired-pulse stimulation. (**b**) Maps of aggregate release probabilities for pulses 1 and 2 ($n = 105$ paired-pulse stimulation trials). Yellow arrowhead, site with a large increase in probability (see Supplementary Fig. 4 for example of a site with a large decrease in probability). Proximal and distal boutons in **a** and **b**, white arrow and asterisk, respectively (two distal boutons are present in the NMJ). Scale bar, 5 μm (**a,b**). (**c**) Change in release probability of individual sites (difference in probabilities between pulses 2 and 1) versus pulse 1 probability. Higher-probability sites tend to depress, whereas lower-probability sites tend to facilitate ($n = 458$ release sites in 7 NMJs, $r = -0.52$; $P < 0.0001$, correlation analysis). (**d**) Distributions of Δ*F/F* values of pulses 1 and 2. $n = 4{,}647$, 6,115 and 351 for pulse 1 (blue), pulse 2 only (magenta, pulse 2 Δ*F* spots at locations that did not respond to pulse 1) and pulse 2 after pulse 1 (green, pulse 2 Δ*F* spots at same site as pulse 1 Δ*F* spots), respectively. Median values ± s.e.m. were: pulse 1, 0.157 ± 0.001; pulse 2 only, 0.1548 ± 0.0008 (distribution not significantly different from that of pulse 1; $P = 0.18$, Kolmogorov-Smirnov test); pulse 2 after pulse 1, 0.146 ± 0.003 (small significant difference from pulse 1 distribution; $P = 0.0005$, Kolmogorov-Smirnov test).

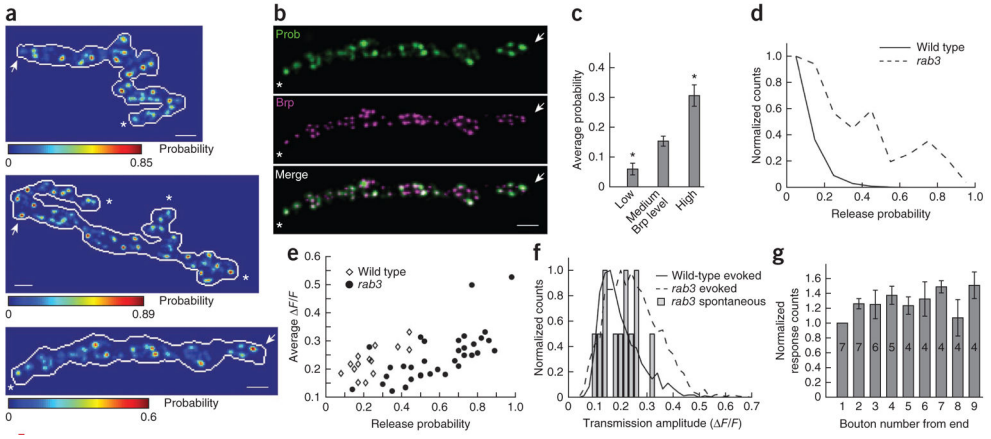

Figure 8.

Transmission properties of *rab3*-mutant NMJs. (**a**) Representative aggregate release probability maps, showing the fraction of times each release site participated in response to nerve stimulation by a single action potential (n = 102, 44 and 96 stimulation trials for top, middle and bottom). (**b**) Comparison of release probability pattern (green, determined by SynapGCaMP2 live imaging) to locations of presynaptically enriched active zones (magenta, confocal image of post-hoc staining for the presynaptic active zone protein Brp) in the NMJ of bottom panel in **a**. Proximal and distal boutons in **a** and **b**, white arrow and asterisk, respectively (middle panel in **a** contains three distal boutons). Scale bar, 5 μm (**a,b**). (**c**) Release probability increases with increasing levels of Brp (n = 198 release sites from 2 NMJs; P < 0.004, independent t-test, comparing medium to low and high Brp levels. See Supplementary Fig. 7 for raw data). (**d**) Distribution of release probabilities in wild-type (n = 495 release sites from 9 NMJs) and *rab3*-mutant (n = 235 release sites from 5 NMJs) NMJs. (**e**) Mean transmission amplitude ($\Delta F/F$ value) is larger for sites of higher release probability in both *rab3*-mutant (n = 35 sites in 4 NMJs, r = 0.68; P < 0.0001, correlation analysis) and wild-type (n = 14 sites in 4 NMJs, r = 0.72; P < 0.004, correlation analysis) NMJs. Only sites that had >9 well-separated ΔF spots were chosen for analysis. (**f**) Distribution of transmission amplitudes ($\Delta F/F$ values) in wild-type (n = 1,096 evoked transmission events from 5 NMJs) and *rab3*-mutant (n = 1,786 evoked transmission events from 4 NMJs, n = 12 spontaneous transmission events from 2 NMJs) NMJs. (**g**) Average number of ΔF spots per bouton (mean ± s.e.m.) versus bouton location from end of branch in *rab3*-mutant NMJs. Counts normalized by bouton area and normalized to distal bouton (bouton number 1). Numbers in bars are number of boutons averaged (n = 7 branches, 5 NMJs).